https://doi.org/10.5194/egusphere-2026-4877
Preprint. Discussion started: 21 September 2026

Sensitivity of NO_2 photolysis frequency to aerosol optical properties

Xinlei Lv[1], Jie Sun[1], Bishuo He[2], Fengjun Shen[1], Gang Zhao[1,*], Tong Liu[1], Qiqi Mo[1], Linghan Zeng[3], Ziye Zhang[1], Yunxiao Li[1], Batu Alaxi[1], Weili Lin[1], Chunsheng Zhao[4]

[1]Key Laboratory of Ecology and Environment in Minority Areas, Minzu University of China, National Ethnic Affairs Commission, Beijing 100081, China
[2]Shanghai Aircraft Flight Test Co., Ltd., Shanghai 201324, China
[3]State Key Laboratory of Atmospheric Environment and Extreme Meteorology, Institute of Atmospheric Physics, Chinese Academy of Sciences, Beijing 100029, China
[4]Department of Atmospheric and Oceanic Sciences, School of Physics, Peking University, Beijing 100871, China

Correspondence to: Gang Zhao (gangz@muc.edu.cn)

Abstract

The photolysis frequency of nitrogen dioxide (NO_2), J(NO_2), links aerosol radiative effects with near-surface photochemistry and ozone formation. Its response to aerosol optical properties is difficult to quantify because scattering, absorption, hygroscopic growth, black carbon coating properties, aerosol vertical distribution, and surface reflection are coupled. We developed a framework combining Mie calculations, the Constrained Parameter (CP) method, and the Tropospheric Ultraviolet and Visible (TUV) model to quantify sensitivities and interactions controlling J(NO_2) using inputs representative of northern China. Two pathways were examined: direct perturbation of aerosol optical depth (AOD), single-scattering albedo (SSA), the asymmetry factor (g), and surface albedo in TUV, and a microphysical pathway in which AOD, SSA, and g were derived from aerosol microphysical parameters using Mie calculations. Among direct radiative inputs, SSA and surface albedo showed the largest CP sensitivities, approximately 12.0×10^{-3} and 5.3×10^{-3} dJ/(dx/x), respectively, indicating stronger control by scattering–absorption partitioning and the lower radiative boundary than by column extinction alone. In the microphysical analysis, coating thickness, black carbon density, black carbon absorption enhancement (BCAE), the imaginary part of the black carbon refractive index, hygroscopicity, and surface albedo were key factors. Interaction and fixed-factor analyses showed that sensitivity rankings were state dependent. The strongest interaction occurred between coating thickness and BCAE. Better constraints on SSA, surface albedo, coating thickness, BCAE, hygroscopicity, and aerosol vertical distribution are needed to improve photolysis-frequency calculations and assessments of coupled fine particulate matter and ozone pollution.

https://doi.org/10.5194/egusphere-2026-4877
Preprint. Discussion started: 21 September 2026

1 Introduction

Synthetic pollution involving fine particulate matter ($PM_{2.5}$) and ozone (O_3) remains a major challenge for air-quality management. Although $PM_{2.5}$ pollution has been substantially reduced in China, O_3 pollution has remained high or has increased in several regions, making coordinated $PM_{2.5}$–O_3 control an important scientific and policy issue (Ma et al., 2021; Liu et al., 2024; He et al., 2024). Aerosols play an important role in this coupled pollution system. On the one hand, aerosols contribute directly to $PM_{2.5}$ mass concentration and further affect particulate pollution (Huang et al., 2014; An et al., 2019). On the other hand, aerosols can modify solar radiation and actinic flux, thereby changing photolysis frequencies and further affecting near-surface photochemistry and O_3 formation (Gerasopoulos et al., 2012; Wang et al., 2019; Zhao et al., 2021).

The photolysis frequency of nitrogen dioxide, $J(NO_2)$, is a central parameter in tropospheric photochemistry and plays an important role in regulating ozone formation and atmospheric oxidizing capacity. NO_2 photolysis produces NO and O^3P, and O^3P subsequently reacts with O_2 to form O_3. Therefore, $J(NO_2)$ directly participates in the NO–NO_2–O_3 cycle (Trebs et al., 2009; Zhao et al., 2021). In general, $J(NO_2)$ is determined by the NO_2 absorption cross section, photolysis quantum yield, and actinic flux. Among these terms, actinic flux is the factor most directly affected by atmospheric radiative conditions, including solar zenith angle, clouds, aerosols, gaseous absorption, surface albedo, ozone column abundance, and altitude (Shetter et al., 2003; Walker et al., 2022).

Aerosols can modify actinic flux by scattering and absorbing ultraviolet and visible radiation before it reaches the near-surface atmosphere, thereby changing $J(NO_2)$ and subsequent O_3 production. Variations in $J(NO_2)$ driven by aerosols and atmospheric conditions have been investigated in different environments, reflecting the importance of photolysis processes in near-surface photochemistry and ozone formation. Long-term measurements in the eastern Mediterranean showed that $J(NO_2)$ varied with aerosol loading, solar zenith angle, and other atmospheric conditions, indicating that aerosols can modify near-surface photolysis conditions (Gerasopoulos et al., 2012). In Beijing, observations and parameterized calculations during 2012–2015 showed that aerosols reduced seasonal mean $J(NO_2)$ by approximately 24% in summer and 30% in winter relative to aerosol-free conditions, and photochemical box-model simulations further indicated that aerosol light extinction reduced the monthly mean daytime net O_3 production rate by up to 25% (Wang et al., 2019). At a suburban site in North China, long-term reconstructed $J(NO_2)$ data from 2005 to 2019 showed that the annual mean aerosol optical depth (AOD) attenuation effect on $J(NO_2)$ was −28.6% relative to an aerosol-free atmosphere, with seasonal mean effects of −27.1%, −35.1%, −25.5%, and −26.3% in spring, summer, autumn, and winter, respectively (Zhao et al., 2021). Model sensitivity experiments further showed that black carbon (BC) aerosols can reduce boundary-layer $J(NO_2)$ by 10%–30% and ground-level O_3 by 5%–20% under highly polluted conditions (Li et al., 2005). These studies demonstrate that aerosol-induced changes in photolysis can propagate into near-surface O_3 production.

AOD, single-scattering albedo (SSA), and the asymmetry factor (g) are key radiative parameters that describe how aerosols affect $J(NO_2)$. AOD controls the magnitude of aerosol extinction and generally reduces near-surface actinic flux under different polluted conditions. Long-term measurements in the eastern Mediterranean showed that AOD averaged over five years of 0.27

https://doi.org/10.5194/egusphere-2026-4877
Preprint. Discussion started: 21 September 2026

± 0.13 reduced $J(NO_2)$ by 5%–14% at a solar zenith angle of 60°, while high aerosol loads with AOD values of 0.5–0.7 reduced photolysis frequencies by up to 30%–40% (Gerasopoulos et al., 2012). SSA determines the partitioning between scattering and absorption, thereby affecting whether aerosols mainly enhance diffuse radiation or attenuate actinic flux through absorption. Aerosol hygroscopic growth can modify wet particle size and SSA, leading to different aerosol effects on $J(NO_2)$; for example, Tao et al. (2014) reported that aerosol hygroscopic growth generally inhibited near-surface $J(NO_2)$ but increased $J(NO_2)$ by 30.4% at 1 km under a relative humidity (RH) of 98%. Absorbing aerosols can further reduce near-surface actinic flux and photolysis rates, with recent AERONET-based calculations over East Asia showing average decreases in $J(NO_2)$ of 16.95% at Chinese sites and 14.90% and 13.71% in the Beijing–Tianjin–Hebei (BTH) and Yangtze River Delta (YRD) regions, respectively (Chen et al., 2023). g characterizes the angular distribution of scattered radiation and affects how aerosol scattering redistributes radiation within the atmosphere. Different aerosol types, with contrasting scattering–absorption characteristics, can therefore affect photolysis rates and O_3 formation in different ways (Gao et al., 2023). In addition to aerosol optical properties, surface albedo regulates the lower radiative boundary by controlling surface reflection, thereby influencing near-surface actinic flux and $J(NO_2)$. Walker et al. (2022) showed that high surface albedo conditions such as snow cover enhanced upwelling diffuse radiation and made the adjustment factor derived from total radiation approximately 40% larger than that derived from downward radiation alone.

Basically, AOD, SSA and g are controlled by aerosol microphysical properties and vertically environmental conditions. Particle number size distribution (PNSD), black-carbon particle number size distribution (BCPNSD), complex refractive indices, black-carbon density (ρ_{BC}), coating thickness (CT), black carbon absorption enhancement (BCAE), mixing state (MS), hygroscopicity (κ), RH, and vertical distribution (VD) can jointly influence aerosol extinction, scattering, absorption, SSA, and g through Mie-based optical calculations and radiative-transfer processes (Tao et al., 2014; Liu et al., 2017; He and Zhao, 2025). For BC-containing aerosols, light absorption depends on coating conditions, MS, particle morphology, and particle-scale heterogeneity. Observational and modelling studies have shown that absorption predicted by idealized core–shell Mie representations can differ from atmospheric measurements because real BC-containing particles do not fully conform to assumptions of concentric spherical geometry, uniform coatings, and homogeneous mixing (Cappa et al., 2012; Fierce et al., 2016; Liu et al., 2017; Lan et al., 2024; Zeng et al., 2024). At present, however, no generally accepted quantitative relationship links the full set of these microphysical properties to the absorption variability that remains unresolved by the idealized core–shell Mie representation. This provides the rationale for including BCAE as a separately prescribed scaling input in the present framework, following He and Zhao (2025). Aerosol hygroscopic growth is also jointly controlled by κ and RH, and it changes particle size and SSA and modifies the vertical dependence of aerosol effects on $J(NO_2)$ (Tao et al., 2014). VD provides another important source of state dependence: observational constraints on vertical aerosol profiles over North China increased surface $J(NO_2)$ by 63.4% in winter and by 33.4%–34.8% in summer, and weakened the default aerosol–photolysis interaction effect on O_3 by 36%–56% (Chen et al., 2025). These findings indicate that the sensitivity of $J(NO_2)$ to a single factor may depend on the states of other factors, leading to nonlinear responses and interaction effects.

https://doi.org/10.5194/egusphere-2026-4877
Preprint. Discussion started: 21 September 2026

Sensitivity analysis provides a general framework for identifying influential input factors and quantifying how input uncertainties or perturbations are transferred to model outputs. In aerosol and radiation studies, one-at-a-time (OAT) perturbation experiments, radiative perturbation experiments, Monte Carlo uncertainty propagation, Morris screening, and variance-based global methods such as Sobol and EFAST have been widely used to evaluate the sensitivity of radiative forcing or radiative fluxes to aerosol and surface parameters (Morris, 1991; Saltelli et al., 1999, 2005; Frey and Patil, 2002; McComiskey et al., 2008; Loeb and Su, 2010; Lee et al., 2011, 2016; Thorsen et al., 2020). These studies commonly focused on parameters such as AOD, SSA, g, VD, cloud conditions, and surface albedo, and they have shown that uncertainties in aerosol optical properties can substantially affect simulated radiation-related quantities.

For photolysis studies, most existing sensitivity or perturbation analyses have evaluated aerosol effects on $J(NO_2)$ within an OAT or OAT-type framework by perturbing aerosol loading, aerosol optical properties, aerosol type, aerosol hygroscopic growth, or VD separately. Early sensitivity analysis showed that $J(NO_2)$ is sensitive to aerosol optical properties, with the strongest response associated with urban aerosols, followed by rural, desert, and maritime aerosols (He and Carmichael, 1999). Model sensitivity experiments further showed that BC aerosols can reduce boundary-layer $J(NO_2)$ by 10%–30% under highly polluted conditions (Li et al., 2005). Observation-based parameterization in Beijing showed that aerosol extinction reduced seasonal mean $J(NO_2)$ by approximately 24% in summer and 30% in winter relative to aerosol-free conditions (Wang et al., 2019). Recent observation–simulation analysis further characterized long-term changes in $J(NO_2)$ in Beijing and explored the influence of aerosols on photolysis rates (Li et al., 2025). At a suburban site in North China, long-term reconstructed $J(NO_2)$ data showed that the annual mean AOD attenuation effect on $J(NO_2)$ was −28.6% during 2005–2019, with the strongest seasonal effect in summer (−35.1%) (Zhao et al., 2021). Recent studies further demonstrated that aerosol type and VD can modify photolysis rates and simulated photochemical responses; for example, observational constraints on aerosol vertical profiles over North China increased surface $J(NO_2)$ by 63.4% in winter and by 33.4%–34.8% in summer (Gao et al., 2023; Chen et al., 2025). These studies indicate that aerosol perturbations can substantially modify $J(NO_2)$, but most of them still quantify the effects of individual factors separately rather than explicitly resolving multi-factor interactions.

However, the OAT or OAT-type framework has inherent limitations for a multi-factor photolysis system. By varying one factor while fixing the others, it mainly represents the local response around a selected reference state and cannot fully capture the co-variation and interaction among aerosol microphysical parameters, environmental conditions, and radiative-boundary factors. This limitation is particularly important for $J(NO_2)$ calculations, because the effect of one factor, such as AOD, SSA, RH, CT, BCAE, VD, or surface albedo, may be amplified, weakened, or even reversed by the states of other factors. At present, quantitative studies that explicitly isolate the interaction effects of these factors on $J(NO_2)$ remain limited. As a result, the apparent sensitivity ranking may misrepresent the real controlling mechanisms of photolysis-frequency changes, and the key parameter combinations that should be prioritized in observations, laboratory measurements, and model constraints remain unclear. More importantly, this uncertainty can propagate into the assessment of aerosol–photochemistry feedbacks and bias

https://doi.org/10.5194/egusphere-2026-4877
Preprint. Discussion started: 21 September 2026

the interpretation of how $PM_{2.5}$ reduction or aerosol-property changes influence near-surface O_3 formation under coordinated $PM_{2.5}$–O_3 control.

The Constrained Parameter (CP) method provides a quantitative approach for evaluating factor sensitivity and interaction effects in multi-factor systems (He and Zhao, 2025). In this method, an unconstrained Monte Carlo simulation is first performed with all input factors varying within their prescribed ranges. A second simulation is then conducted by constraining the range of one target factor while retaining the variability of the other factors. The change in the output distribution is used to quantify the sensitivity of the target factor. By comparing CP-based sensitivities with OAT-based sensitivities, the contribution from factor interactions can also be diagnosed. This method was originally developed to quantify uncertainty contributions in aerosol–radiation interactions, and its logic provides a suitable basis for evaluating how aerosol optical properties, aerosol microphysical parameters, environmental conditions, and radiative-boundary effects jointly influence $J(NO_2)$.

This study develops a coupled Mie and Tropospheric Ultraviolet and Visible (TUV) framework that incorporates the CP method to evaluate the sensitivity and interaction effects of aerosol and environmental factors on $J(NO_2)$ near the surface. Using this framework, we first quantify the sensitivities of $J(NO_2)$ to direct radiative inputs, including AOD, SSA, g, and surface albedo, and examine whether their effects are independent or modulated by factor interactions. We then extend the analysis to aerosol microphysical parameters and environmental conditions, including PNSD, BCPNSD, complex refractive indices, ρ_{BC}, MS, CT, BCAE, κ, RH, and VD, to determine how these factors affect $J(NO_2)$ through changes in aerosol optical properties and actinic flux. In addition, a pairwise CP-based interaction analysis is developed to quantify the interaction effect between two selected factors, and fixed-factor experiments are further used to examine how the sensitivity of $J(NO_2)$ changes under different parameter states. Through these analyses, this study identifies the key aerosol-related parameters and parameter combinations that should be better constrained in photolysis-frequency calculations. The results provide a quantitative basis for improving the representation of aerosol–photochemistry interactions in assessments of coupled $PM_{2.5}$–O_3 pollution. Section 2 describes the data and methods, Sect. 3 presents the sensitivity and interaction results, and Sect. 4 summarizes the main conclusions and limitations.

https://doi.org/10.5194/egusphere-2026-4877
Preprint. Discussion started: 21 September 2026

2 Methods

2.1 Mie model

Mie theory was used to calculate aerosol optical properties from aerosol microphysical parameters (Bohren and Huffman, 1983). For a given wavelength, particle size, complex refractive index, and mixing structure, the Mie calculation yields the extinction efficiency, scattering efficiency, absorption efficiency, and single-particle asymmetry factor.

For BC-containing particles, a uniform core–shell structure was assumed. The BC core was treated as the light-absorbing component and was described by the BC particle size, ρ_{BC}, and complex refractive index of BC, whereas the shell represented the coating material and was described by CT and shell refractive index (He and Zhao, 2025).

Aerosol hygroscopic growth was treated using the κ-Köhler growth factor (Petters and Kreidenweis, 2007). For a dry particle with diameter $D_{p,dry}$, the wet particle diameter was calculated as:

$$D_{p,wet} = D_{p,dry} \cdot GF \tag{1}$$

where the hygroscopic growth factor GF was calculated as:

$$GF = \left(1 + \kappa \frac{RH}{1-RH}\right)^{1/3} \tag{2}$$

During aerosol hygroscopic growth, the BC core diameter and BC complex refractive index were kept unchanged, whereas water uptake was assumed to occur in the shell. The wet shell complex refractive index was obtained by volume-weighted mixing of the dry shell material and water, following the treatment used by He and Zhao (2025).

For each particle diameter D_p and wavelength λ, the extinction, scattering, and absorption cross sections were calculated as:

$$C_{ext}(D_p, \lambda) = \frac{\pi D_p^2 Q_{ext}(D_p, \lambda)}{4} \tag{3}$$

$$C_{sca}(D_p, \lambda) = \frac{\pi D_p^2 Q_{sca}(D_p, \lambda)}{4} \tag{4}$$

$$C_{abs}(D_p, \lambda) = C_{ext}(D_p, \lambda) - C_{sca}(D_p, \lambda) \tag{5}$$

where Q_{ext}, Q_{sca}, and Q_{abs} are the extinction, scattering, and absorption efficiencies, respectively.

The single-particle optical properties were then integrated over the particle population to derive bulk aerosol optical properties. PNSD and BCPNSD were used as size-resolved inputs to describe the total aerosol particle population and the BC-containing particle population, respectively. The extinction and scattering coefficients were calculated as:

$$b_{ext}(\lambda, z) = \int C_{ext}(D_p, \lambda, z) n(D_p, z)\, dD_p \tag{6}$$

$$b_{sca}(\lambda, z) = \int C_{sca}(D_p, \lambda, z) n(D_p, z)\, dD_p \tag{7}$$

where $n(D_p, z)$ is the PNSD at height z. The absorption coefficient was calculated as:

$$b_{abs}(\lambda, z) = b_{ext}(\lambda, z) - b_{sca}(\lambda, z) \tag{8}$$

https://doi.org/10.5194/egusphere-2026-4877
Preprint. Discussion started: 21 September 2026

The bulk SSA was calculated as:

$$SSA(\lambda, z) = \frac{b_{sca}(\lambda, z)}{b_{ext}(\lambda, z)} \quad (9)$$

The bulk asymmetry factor was calculated as the scattering-weighted mean of the single-particle asymmetry factor:

$$g(\lambda, z) = \frac{\int g_p(D_p, \lambda, z) C_{sca}(D_p, \lambda, z) n(D_p, z)\, dD_p}{\int C_{sca}(D_p, \lambda, z) n(D_p, z)\, dD_p} \quad (10)$$

AOD was obtained by vertically integrating the extinction coefficient:

$$AOD(\lambda) = \int b_{ext}(\lambda, z)\, dz \quad (11)$$

In this formulation, PNSD, BCPNSD, n_{BC}, k_{BC}, n_{Shell}, ρ_{BC}, CT, and MS defined the particle population and core–shell microphysical state used in the Mie-based optical calculation. Following He and Zhao (2025), BCAE was included as a separately prescribed, dimensionless model input used to scale the Mie-derived absorption of the internally mixed core–shell BC-containing fraction. For each sampled set of microphysical inputs, the Mie model first calculated the scattering and absorption efficiencies. The Mie-derived absorption efficiency of the BC-containing fraction was then scaled by BCAE, while the Mie-derived scattering efficiency remained unchanged. The extinction efficiency was obtained as the sum of the unchanged scattering efficiency and the scaled absorption efficiency. The particle-level optical contributions were subsequently integrated over PNSD and BCPNSD to obtain the bulk scattering, absorption, and extinction coefficients. SSA was calculated from the bulk scattering and extinction coefficients, and g was obtained as the scattering-weighted mean of the single-particle asymmetry factor. In the sensitivity analysis, BCAE was varied as a separate input factor; consequently, the scaled absorption was jointly determined by BCAE and the sampled core–shell microphysical state. The κ and RH values were used to account for aerosol hygroscopic growth before the optical calculation. VD was not used in the single-particle Mie calculation. After the Mie-based optical calculation, the bulk extinction coefficient was combined with the prescribed VD to obtain layer aerosol optical depths, which were subsequently supplied to TUV. The Mie calculations were implemented in Python using the PyMieScatt package (v1.8.1.1). The factor settings and input structure were based on the data framework of He and Zhao (2025), and the specific parameter settings are listed in Sect. 2.3.

2.2 TUV model

The TUV radiative-transfer model was used to calculate the near-surface $J(NO_2)$ (Madronich and Flocke, 1999). This study used a Mie–TUV framework in which Mie-derived aerosol optical properties were supplied to the radiative-transfer model, with $J(NO_2)$ as the target output. TUV calculates wavelength-dependent actinic flux under prescribed solar geometry, atmospheric absorption, aerosol optical properties, VD, and surface reflection. Cloud-free conditions were used to isolate the effects of aerosol-related and environmental factors on $J(NO_2)$.

The photolysis frequency of NO_2 was calculated as:

$$J(NO_2)(z, t) = \int \sigma_{NO_2}(\lambda, T) \Phi_{NO_2}(\lambda, T) F(\lambda, z, t)\, d\lambda \quad (12)$$

https://doi.org/10.5194/egusphere-2026-4877
Preprint. Discussion started: 21 September 2026

where $\sigma_{NO_2}(\lambda, T)$ is the NO_2 absorption cross section, $\Phi_{NO_2}(\lambda, T)$ is the NO_2 photolysis quantum yield, and $F(\lambda, z, t)$ is the actinic flux at wavelength λ, height z, and time t. The integration was performed over the wavelength range relevant to NO_2 photolysis. The NO_2 absorption cross section and quantum yield were taken from the JPL evaluation 19 (Burkholder et al., 2019), and the output at the lowest model layer was used to represent near-surface $J(NO_2)$.

The TUV inputs relevant to aerosol radiative effects included AOD, SSA, g, surface albedo, VD, the extinction Ångström exponent (α_{ext}), and the absorption Ångström exponent (AAE). The observation-derived SSA at 525 nm (SSA_{525}) constrained the partitioning between aerosol scattering and absorption at the reference wavelength. Following established Ångström power-law representations of aerosol extinction and absorption (Bergstrom et al., 2007; Russell et al., 2010; Moosmüller and Chakrabarty, 2011), α_{ext} and AAE were used to describe their respective wavelength dependences. Together with SSA_{525}, these spectral exponents were used to derive wavelength-dependent SSA over 280–420 nm for the TUV calculation of $J(NO_2)$ (Doherty et al., 2022; Kayetha et al., 2022). The prescribed g controlled the angular redistribution of scattered radiation. Surface albedo provided the lower boundary condition for surface reflection. VD was used to allocate column aerosol extinction to different model layers, so that the vertically integrated aerosol extinction was consistent with the prescribed AOD. Although only near-surface $J(NO_2)$ was analyzed, VD was included because it affects the actinic flux reaching the near-surface layer.

Two calculation pathways were used. In the direct radiative-input pathway, AOD, SSA, g, and surface albedo were treated as the sensitivity-analysis variables. AAE and α_{ext} were supplied as background spectral inputs in each TUV calculation. In the microphysical pathway, aerosol microphysical and environmental inputs were first used in the Mie-based optical calculations. As described in Sect. 2.1, BCAE was included as a separately prescribed input used to scale the Mie-derived absorption of the BC-containing fraction, and the resulting scattering and absorption contributions were integrated to obtain the bulk aerosol extinction, scattering, and absorption coefficients, SSA, and g. The calculated extinction coefficient was then combined with the prescribed VD to obtain layer aerosol optical depths. These layer aerosol optical depths, together with SSA, g, and surface albedo, were supplied to TUV as layer-resolved aerosol optical inputs for calculating actinic flux and $J(NO_2)$. This pathway was used to evaluate how aerosol microphysical and environmental factors influence $J(NO_2)$ through their effects on aerosol optical properties.

The TUV calculations were performed using TUV version 5.3. The model was configured with the site information, date, solar geometry, gas column settings, aerosol optical inputs, surface albedo, and vertical grid settings listed in Sect. 2.3. The overall workflow was as follows: when required, aerosol microphysical inputs and the separately prescribed BCAE scaling input were used in the Mie-based optical calculation to obtain the bulk extinction coefficient, SSA, and g; the extinction coefficient was then combined with VD to obtain layer aerosol optical depths, which were supplied to TUV together with SSA, g, and surface albedo to calculate wavelength-dependent actinic flux; finally, $J(NO_2)$ was obtained by integrating the product of actinic flux, the NO_2 absorption cross section, and the quantum yield over wavelength. The detailed implementation of the CP sensitivity analysis was based on He and Zhao (2025) and is described in Sect. 2.5.

https://doi.org/10.5194/egusphere-2026-4877
Preprint. Discussion started: 21 September 2026

2.3 Data sources

The input data used in this study were organized according to the two calculation pathways described in Sect. 2.2. The direct radiative-input dataset included AOD, SSA, g, surface albedo, AAE, and α_{ext}, which were supplied to TUV. The aerosol microphysical and environmental dataset was adapted from the publicly available supporting data of He and Zhao (2025) and reorganized for the Mie–TUV calculation of $J(NO_2)$. This dataset included PNSD, BCPNSD, refractive indices, ρ_{BC}, CT, BCAE, MS, κ, RH, VD, and surface albedo.

AOD and surface albedo were obtained from MODIS products (Levy et al., 2013; Schaaf et al., 2002). The scattering and absorption coefficients used to calculate SSA were obtained from observations at the Peking University Changping site. Because aerosol scattering was measured at 525 nm and the nearest available absorption channel was 520 nm, SSA at 525 nm was approximated as:

$$SSA_{525} = \frac{b_{sca,525}}{b_{sca,525} + b_{abs,520}} \tag{13}$$

where $b_{sca,525}$ and $b_{abs,520}$ denote the scattering coefficients at 525 nm and the absorption coefficient at 520 nm, respectively. g was constrained following the aerosol optical parameterization of Zhao et al. (2018). The site information, simulation date, wavelength range, gas column settings, aerosol optical inputs, surface albedo, and vertical grid settings used in TUV are summarized in Table 1.

In the microphysical pathway, PNSD and BCPNSD were used to describe the size-resolved aerosol and BC-containing particle populations. Refractive indices and ρ_{BC} defined the optical response of BC-containing particles. CT and MS described the prescribed BC coating thickness and mixing state, respectively, whereas BCAE was included as a separately prescribed, dimensionless scaling input used to scale the Mie-derived absorption of the BC-containing fraction for each sampled core–shell microphysical state, as described in Sect. 2.1. κ and RH were used to account for hygroscopic growth before the Mie calculation. VD was used to distribute aerosol extinction with height before the TUV calculation.

Table 1 summarizes the sensitivity-analysis parameters and main model settings used in the direct radiative-input and microphysical analyses. For scalar variables, the representative value or uncertainty range is given directly. For size-resolved or height-resolved variables, such as PNSD, BCPNSD, CT, BCAE, RH, and VD, " / " is used in the table because these inputs are multi-dimensional arrays rather than single scalar values. The original size-resolved and profile-resolved data were used in the calculations.

Based on the above input configuration and modelling framework, the simulations were performed as follows. For the direct radiative-input analysis, AOD, SSA, g, and surface albedo were prescribed directly in TUV together with the model settings listed in Table 1 to calculate near-surface $J(NO_2)$. For the microphysical analysis, the microphysical inputs, κ, RH, and the separately prescribed BCAE scaling input were used in the Mie-based optical calculation to obtain the bulk extinction coefficient, SSA, and g. The extinction coefficient was then combined with VD to obtain layer aerosol optical depths, which were supplied to TUV together with SSA, g, and surface albedo to calculate near-surface $J(NO_2)$. The sensitivity-analysis

https://doi.org/10.5194/egusphere-2026-4877
Preprint. Discussion started: 21 September 2026

procedures were then applied to the corresponding input variables, while the detailed CP implementation followed He and Zhao (2025).

https://doi.org/10.5194/egusphere-2026-4877
Preprint. Discussion started: 21 September 2026

Table 1. Sensitivity-analysis parameters and main model settings used in the direct radiative-input and aerosol microphysical analyses.

Analysis level	Parameter	Meaning	Value or range	Source or setting
Direct radiative input	AOD	Aerosol optical depth	0.2619 ± 0.2411	MODIS
Direct radiative input	SSA_{525}	Single-scattering albedo at 525 nm	0.9200 ± 0.0470	Changping observations
Direct radiative input	g	Aerosol asymmetry factor	0.6390 ± 0.0490	Zhao et al. (2018)
Radiative boundary condition	Surface albedo	Surface reflectance	0.1425 ± 0.0010	MODIS
Model setting	Location	Simulation site	40.2457° N, 116.1934° E; 92 m a.s.l.	Peking University Changping site
Model setting	Date and time	Simulation time	1 May, local noon	This study
Model setting	Wavelength range	Spectral range for $J(NO_2)$ calculation	280–420 nm	TUV setting
Aerosol microphysical factor	PNSD	Particle number size distribution	/	He and Zhao (2025)
Black-carbon microphysical factor	BCPNSD	Black-carbon particle number size distribution	/	He and Zhao (2025)
Aerosol optical factor	n_{shell}	Real part of shell refractive index	1.58 ± 0.20	He and Zhao (2025)
Black-carbon optical factor	n_{BC}	Real part of BC refractive index	1.67 ± 0.36	He and Zhao (2025)
Black-carbon optical factor	k_{BC}	Imaginary part of BC refractive index	0.67 ± 0.35	He and Zhao (2025)
Black-carbon physical factor	ρ_{BC}	Black-carbon density	0.95 ± 0.30	He and Zhao (2025)
Mixing-state factor	MS	Aerosol mixing state	0.70 ± 0.30	He and Zhao (2025)
Coating factor	CT	Coating thickness	/	He and Zhao (2025)
BC absorption-enhancement factor	BCAE	Black-carbon absorption enhancement	/	He and Zhao (2025)
Hygroscopic factor	κ	Hygroscopicity parameter	0.22 ± 0.20	He and Zhao (2025)
Environmental factor	RH	Relative humidity	/	He and Zhao (2025)
Vertical-structure factor	VD	Aerosol vertical distribution	/	He and Zhao (2025)

Note: " / " indicates that the corresponding values are two-dimensional or higher-dimensional inputs and therefore cannot be represented by a single scalar in the table. Detailed data for these inputs are available from the public data support of the previous study (He and Zhao, 2025).

https://doi.org/10.5194/egusphere-2026-4877
Preprint. Discussion started: 21 September 2026

2.4 OAT sensitivity analysis

The OAT method was used as the conventional local sensitivity analysis. In OAT, one input factor was perturbed while all other factors were fixed at their reference values. For a multi-factor system, the model output can be expressed as:

$$Y = f(X), X = [x_1, x_2, \cdots, x_n]^{\mathrm{T}} \quad (14)$$

where Y represents the model output and X is the vector of input factors. In this study, Y is the NO_2 photolysis frequency $J(NO_2)$. Around a selected reference state A, the local response of f(X) to the ith factor can be described by the first-order derivative:

$$S_{i,OAT} = \left(\frac{\partial f(X)}{\partial x_i}\right)_{X \to A} \quad (15)$$

For the present application, this sensitivity is written as:

$$S_{i,OAT} = \frac{dJ(NO_2)}{dx_i} \quad (16)$$

The OAT method is computationally efficient and intuitive because it directly evaluates the response of $J(NO_2)$ to a selected factor. However, because the other factors are fixed during each perturbation, OAT represents a local response around the selected background state and does not explicitly quantify factor interactions.

2.5 CP method

CP method was applied following a previously developed framework (He and Zhao, 2025). In CP method, an unconstrained Monte Carlo simulation is first performed with all input factors varying within their prescribed ranges. A second Monte Carlo simulation is then conducted by constraining the range of one target factor x_i, while the ranges of the other factors are retained. The sensitivity is calculated from the change in the output variance caused by constraining x_i.

If the standard deviation of the model output changes from σ_γ to σ'_γ after constraining x_i, and the standard deviation of x_i changes from σ_{xi} to σ'_{xi}, the CP sensitivity is defined as:

$$S_{i,CP} = \sqrt{\frac{\sigma_Y^2 - \sigma'^2_Y}{\sigma_{x_i}^2 - \sigma'^2_{x_i}}} = \sqrt{\frac{d\sigma_J^2}{d\sigma_{x_i}^2}} \quad (17)$$

In this study, Y corresponds to $J(NO_2)$, so the CP sensitivity can also be written as:

$$S_{i,CP} = \sqrt{\frac{d\sigma_J^2}{d\sigma_{x_i}^2}} \quad (18)$$

Compared with OAT, the CP method evaluates the response of $J(NO_2)$ under simultaneous variations of multiple factors. Therefore, differences between CP and OAT sensitivities provide information on nonlinear responses and factor interactions.

2.6 Pairwise interaction evaluation using the CP method

The interaction associated with each factor was evaluated by comparing OAT and CP sensitivities. The derivation follows a previous interpretation of the CP method (He and Zhao, 2025). The output variance of a multi-factor system can be decomposed

https://doi.org/10.5194/egusphere-2026-4877
Preprint. Discussion started: 21 September 2026

into the contribution from individual factors and the covariance-related contribution from factor interactions. For the model output Y = f(X), the output variance can be expressed as:

$$\sigma_Y^2 = \Sigma_{j=1}^{N} S_j^2 \sigma_{x_j}^2 + \Sigma_{j<k} I_{jk} + \cdots \quad (19)$$

After constraining the range of the target factor x_i, its variance changes from σ_{xi}^2 to σ'^2_{xi}, and the output variance changes from σ_Y^2 to σ'^2_Y. The constrained output variance can be written schematically as:

$$\sigma'^2_Y = \Sigma_{j\neq i} S_j^2 \sigma_{x_j}^2 + S_i^2 \sigma'^2_{x_i} + \Sigma_{j<k} I'_{jk} + \cdots \quad (20)$$

Therefore, the change in output variance caused by constraining x_i is:

$$\Delta\sigma_Y^2 = \sigma_Y^2 - \sigma'^2_Y \quad (21)$$

According to the CP definition:

$$S_{i,CP}^2 = \frac{\Delta\sigma_Y^2}{\sigma_{x_i}^2 - \sigma'^2_{x_i}} \quad (22)$$

The CP sensitivity can therefore be interpreted as the local OAT contribution plus an interaction-related term:

$$S_{i,CP}^2 = S_{i,OAT}^2 + I_i \quad (23)$$

Because the first term corresponds to the local OAT sensitivity:

$$S_{i,OAT} = \frac{\partial f_i(X_i)}{\partial X_i} \quad (24)$$

The interaction-related term can be written as:

$$I_i = S_{i,CP}^2 - S_{i,OAT}^2 \quad (25)$$

This relationship indicates that CP includes both the local single-factor response represented by OAT and the additional contribution associated with factor interaction. When the factors are independent and the model response is approximately linear, the interaction term approaches zero and CP gives the same result as OAT.

Following the plotting treatment used in the previous CP study, this study used the absolute difference between the OAT and CP sensitivities to represent the relative strength of interaction (He and Zhao, 2025). The interaction associated with factor x_i and the other parameters was therefore calculated as:

$$\text{interaction}_i = \left|S_{i,OAT} - S_{i,CP}\right| \quad (26)$$

Pairwise interaction analysis was also used to identify factor combinations with stronger interaction, following the same CP–OAT comparison framework. For the pairwise analysis, two factors were constrained together and the resulting change in CP sensitivity was compared with the corresponding OAT-based response, so as to identify factor pairs with stronger joint effects on $J(NO_2)$. No additional two-factor formula was introduced in the main text; the analysis was interpreted consistently with the CP-OAT interaction framework described above.

Fixed-factor experiments were further conducted to examine whether the sensitivity ranking depended on the background state of key factors. Surface albedo, CT, BCAE, and κ were fixed at selected levels, and the CP sensitivities of the remaining factors were recalculated. These experiments were used to examine how surface reflection, coating thickness, BCAE, and hygroscopic growth modulate the sensitivity of $J(NO_2)$ to other aerosol-related factors.

https://doi.org/10.5194/egusphere-2026-4877
Preprint. Discussion started: 21 September 2026

3 Results and discussion

3.1 Sensitivity of $J(NO_2)$ to direct radiative inputs

The direct radiative-input analysis was used to identify how AOD, SSA, g, and surface albedo directly affect near-surface $J(NO_2)$ in the TUV calculations. Among these inputs, SSA showed the largest CP sensitivity, approximately 12.0×10^{-3} dJ/(dx/x), followed by surface albedo with a sensitivity of approximately 5.3×10^{-3} dJ/(dx/x) (Fig. 1). The sensitivities of AOD and g were much smaller, both close to 0.8×10^{-3} dJ/(dx/x). This ranking was derived from the CP sensitivity calculation described in Sect. 2.5 and therefore reflects the response of $J(NO_2)$ within the prescribed uncertainty ranges of the direct radiative inputs.

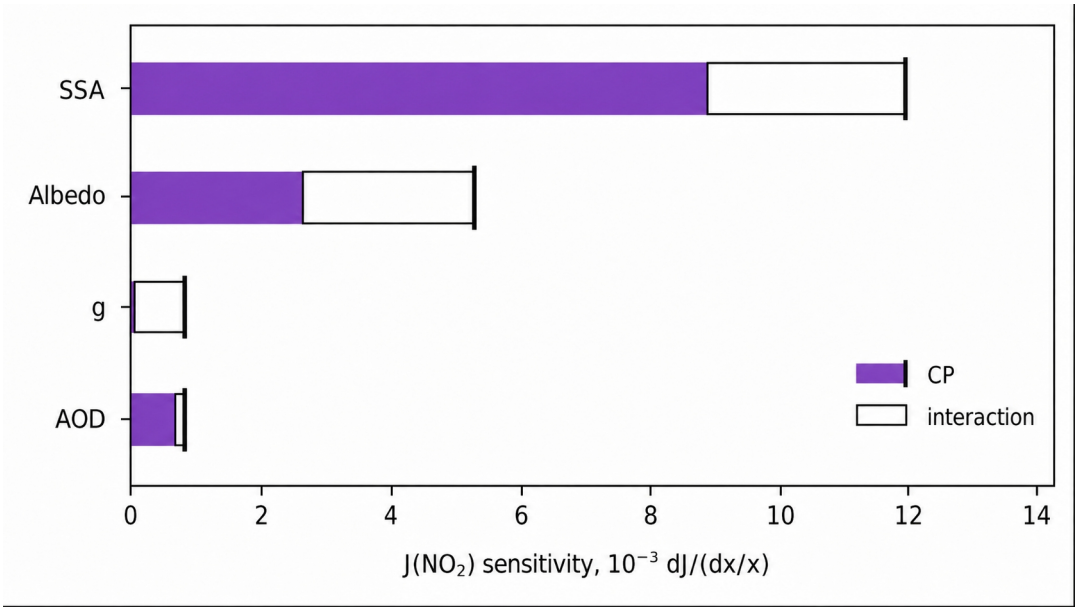

Figure 1. Sensitivity of $J(NO_2)$ to direct radiative inputs. Purple bars together with black vertical lines represent CP sensitivity, and white bars represent interaction. The horizontal-axis unit is 10^{-3} dJ/(dx/x).

The dominant sensitivity to SSA indicates that $J(NO_2)$ is strongly affected by the scattering–absorption partitioning of aerosol extinction. Physically, SSA determines whether aerosol extinction is partitioned mainly into scattering, which can enhance diffuse radiation, or into absorption, which attenuates actinic flux. This interpretation is consistent with previous studies showing that absorbing aerosols can reduce near-surface photolysis frequencies and modify O_3 production, whereas aerosol types with different scattering–absorption characteristics can produce different responses in photolysis rates and ozone formation (Li et al., 2005; Chen et al., 2023; Gao et al., 2023). Therefore, the large SSA sensitivity obtained here is not only a numerical result from the CP analysis but also reflects the physical role of SSA in regulating the actinic-flux field.

Surface albedo also showed a clear influence on $J(NO_2)$. Although surface albedo is not an aerosol optical property, it acts as the lower radiative boundary condition in TUV and regulates multiple scattering between the surface and the atmosphere.

https://doi.org/10.5194/egusphere-2026-4877
Preprint. Discussion started: 21 September 2026

Previous work has shown that high-surface-albedo conditions can enhance upwelling diffuse radiation and affect adjustment factors for photolysis-rate coefficients (Walker et al., 2022). The relatively high sensitivity of surface albedo in this study therefore indicates that aerosol optical effects and surface reflection jointly control near-surface actinic flux.

The smaller sensitivities of AOD and g do not mean that these two parameters are unimportant. AOD has been shown to attenuate $J(NO_2)$ under different polluted conditions, including the eastern Mediterranean, Beijing, and suburban North China (Gerasopoulos et al., 2012; Wang et al., 2019; Zhao et al., 2021). g determines the angular redistribution of scattered radiation and is an important aerosol optical input in radiative-transfer calculations (Zhao et al., 2018). In the present analysis, however, their direct CP sensitivities were lower than those of SSA and surface albedo within the adopted parameter ranges. Since SSA and g are ultimately controlled by aerosol microphysical properties, the following section further examines the aerosol, black-carbon, hygroscopic, environmental, and boundary-condition factors that regulate $J(NO_2)$.

3.2 Sensitivity to aerosol microphysical factors, environmental conditions, and radiative boundary conditions

For aerosol microphysical, environmental, and boundary-condition factors, relatively high CP sensitivities were found for CT, ρ_{BC}, BCAE, surface albedo, k_{BC}, and κ (Fig. 2). This ranking was obtained through the Mie–TUV pathway, in which aerosol microphysical and environmental inputs were first converted into aerosol optical properties and then used to calculate $J(NO_2)$. Therefore, these results indicate which underlying factors most efficiently affect $J(NO_2)$ through changes in extinction, scattering, absorption, SSA, and g.

CT showed the strongest sensitivity among the aerosol microphysical factors. CT represents the prescribed coating thickness of BC-containing particles, and changes in CT can modify BC absorption, scattering, and SSA. Previous measurements and modelling studies have shown that observed BC absorption enhancement varies with MS, coating conditions, and particle-scale heterogeneity (Cappa et al., 2012; Liu et al., 2017; Fierce et al., 2016; Lan et al., 2024; Zeng et al., 2024). These studies provide a physical basis for interpreting the high CT sensitivity found here: coating thickness affects $J(NO_2)$ mainly by altering BC optical properties and the scattering–absorption partitioning represented by SSA.

The relatively large sensitivities of ρ_{BC}, BCAE, and k_{BC} further highlight the importance of BC absorption-related properties. For a given BC mass, ρ_{BC} affects the volume-equivalent BC core size, k_{BC} controls the intrinsic light-absorbing capacity of BC, and BCAE represents the multiplicative enhancement applied to the Mie-calculated BC absorption. These parameters jointly influence the optical properties of BC-containing particles, particularly BC absorption and the scattering–absorption balance, within the Mie-based optical framework. The importance of these BC absorption-related parameters is consistent with earlier model sensitivity experiments showing that BC aerosols can reduce boundary-layer $J(NO_2)$ and influence ground-level O_3 under polluted conditions (Li et al., 2005).

https://doi.org/10.5194/egusphere-2026-4877
Preprint. Discussion started: 21 September 2026

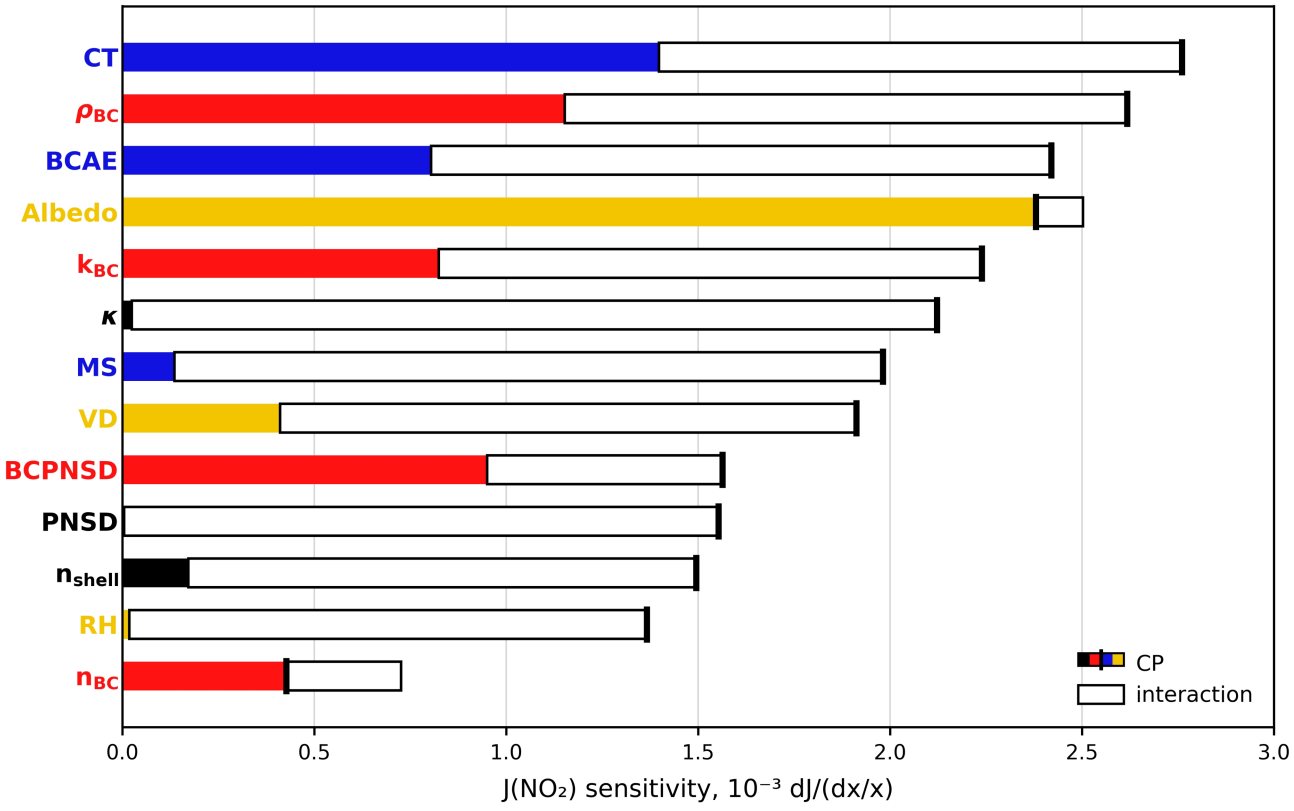

Figure 2. Sensitivity of $J(NO_2)$ to aerosol microphysical factors, environmental conditions, and radiative boundary conditions. Coloured bars together with black vertical lines represent CP sensitivity, and white bars represent interaction. The horizontal-axis unit is 10^{-3} dJ/(dx/x).

κ also showed a clear influence. The parameter κ controls the intrinsic ability of particles to take up water, whereas RH provides the environmental condition for water uptake. According to the κ-Köhler framework, water uptake changes wet particle size and consequently modifies aerosol optical properties (Petters and Kreidenweis, 2007). Tao et al. (2014) further showed that aerosol hygroscopic growth can alter SSA and change the vertical pattern of $J(NO_2)$ responses. Therefore, the sensitivity of $J(NO_2)$ to κ in this study can be understood as the optical consequence of hygroscopic growth, which modifies wet particle size, scattering efficiency, and SSA before the TUV calculation. Surface albedo remained important because it directly controls the lower radiative boundary rather than being derived from the Mie calculation, consistent with the direct-input results and with previous photolysis studies involving surface reflection (Walker et al., 2022).

Some factors, such as PNSD, BCPNSD, n_{shell}, RH, and n_{BC}, showed lower individual CP sensitivities. However, lower individual sensitivity does not necessarily imply a negligible role, because factor interactions and changes in the background state can modify the sensitivity ranking. These effects are further examined through the interaction and fixed-factor analyses in the following sections.

https://doi.org/10.5194/egusphere-2026-4877
Preprint. Discussion started: 21 September 2026

3.3 Influence of factor interactions on the sensitivity ranking

Interaction was evaluated as defined in Sect. 2.6 by comparing OAT and CP sensitivities. The interaction results show that the sensitivity ranking is not only controlled by individual factor effects but also by the coupling among aerosol microphysical properties, environmental conditions, and radiative boundary conditions (Figs. 3 and 4). This interpretation follows the logic of the CP method, in which the difference between the local OAT response and the CP response under simultaneous factor variation is used to diagnose nonlinear responses and factor interactions (He and Zhao, 2025).

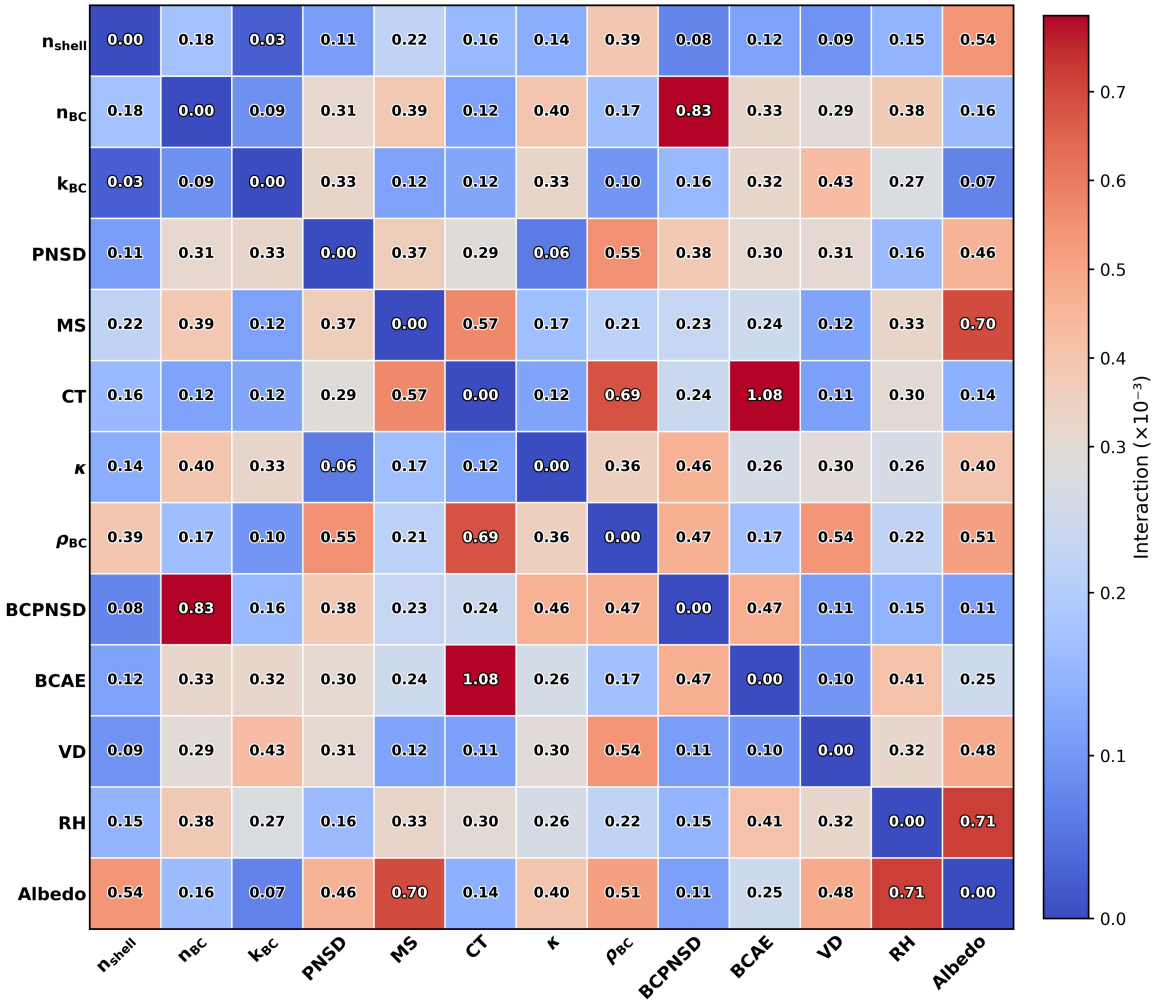

Figure 3. Interaction matrix among aerosol-related factors. Colours represent interaction. Brighter colours indicate stronger interaction.

The strongest interaction occurred between CT and BCAE. This result indicates that CT and BCAE should be considered together when interpreting their combined influence on $J(NO_2)$. This interaction is physically reasonable because CT changes the core–shell optical structure, whereas BCAE independently scales the Mie-calculated BC absorption. Previous studies have

https://doi.org/10.5194/egusphere-2026-4877
Preprint. Discussion started: 21 September 2026

shown that observed BC absorption enhancement varies with coating conditions, MS, and particle-scale heterogeneity (Cappa et al., 2012; Liu et al., 2017; Fierce et al., 2016; Lan et al., 2024; Zeng et al., 2024). Therefore, the strong CT–BCAE interaction obtained here is consistent with the established understanding of BC optical properties and explains why constraining only one of these two parameters may not fully capture their combined influence on $J(NO_2)$.

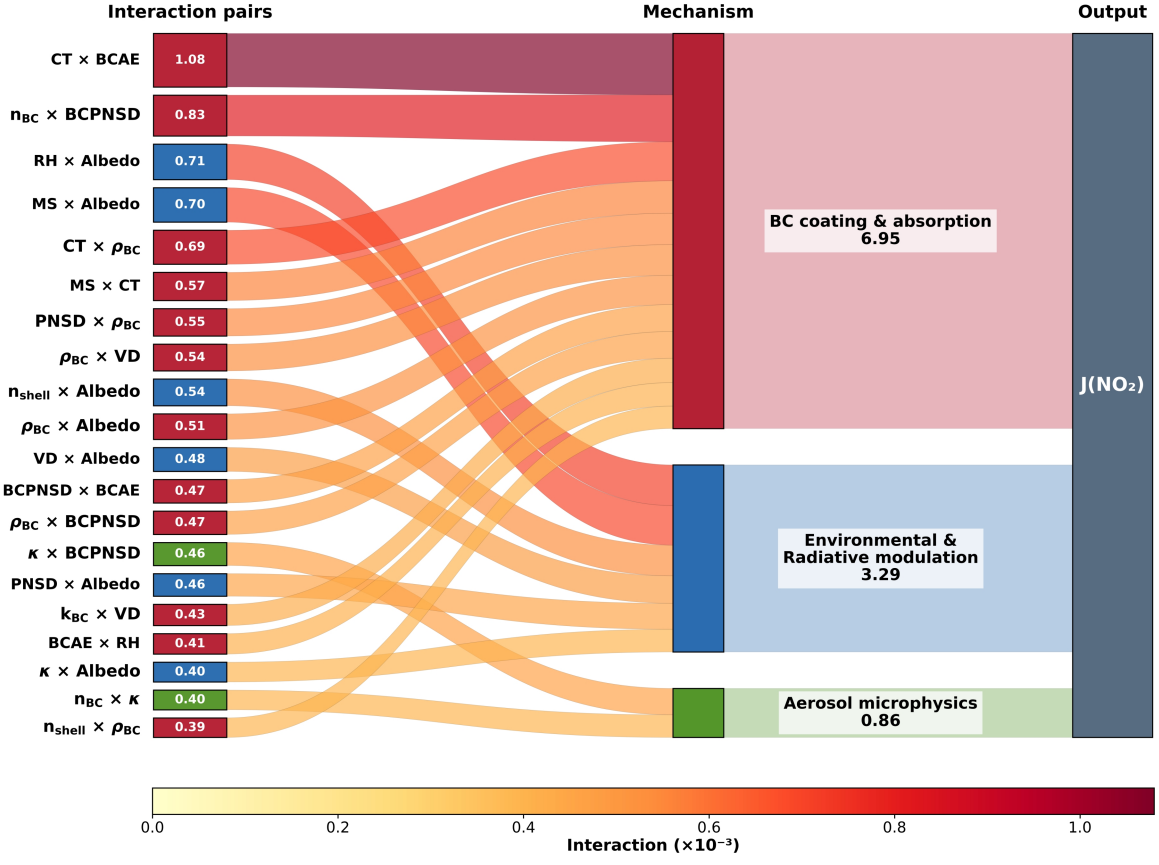

Figure 4. Top 20 interaction pathways among aerosol-related factors and their associated mechanisms. Colours represent interaction, with darker colours indicating stronger interaction.

Other strong interactions involved BC size distribution, BC refractive index, ρ_{BC} and BCAE. These factors jointly influence the optical properties of BC-containing particles, particularly absorption and the scattering–absorption balance, within the Mie-based optical framework. Their interactions explain why several BC-related factors showed clear differences between OAT and CP sensitivities in Fig. 2. In other words, the apparent importance of one BC-related parameter depends on the state of other BC physical and optical parameters. This result is consistent with previous findings that BC absorption and absorption enhancement are sensitive to particle-scale diversity and mixing-state representation (Fierce et al., 2016; Zeng et al., 2024). Surface albedo also interacted with several aerosol and environmental factors. This indicates that the lower radiative boundary condition regulates how aerosol optical perturbations are transferred to near-surface $J(NO_2)$. Under a more reflective surface,

https://doi.org/10.5194/egusphere-2026-4877
Preprint. Discussion started: 21 September 2026

changes in aerosol scattering, absorption, and VD can have different impacts on actinic flux because surface reflection enhances multiple scattering between the surface and the aerosol layer. This mechanism is consistent with the importance of surface reflection in photolysis-rate calculations under high-albedo conditions (Walker et al., 2022).

Interactions involving RH, κ, PNSD, BCPNSD, and MS further show that hygroscopic growth, size distribution, and MS do not act independently. Hygroscopic growth changes wet particle size and SSA, while size distribution controls the weighting of particles that contribute to extinction, scattering, and absorption. Previous studies have shown that hygroscopic growth can strongly modify SSA and $J(NO_2)$, especially under high-RH conditions (Tao et al., 2014), and the κ-Köhler framework provides the physical basis for linking κ to wet particle size (Petters and Kreidenweis, 2007). These results provide a physical basis for the state dependence tested by the fixed-factor experiments in Sect. 3.4.

3.4 CP sensitivity under fixed levels of key factors

To test whether the sensitivity ranking depends on the background state of key factors, fixed-factor experiments were conducted for surface albedo, CT, BCAE, and κ. These factors represent the lower radiative boundary condition, coating thickness, prescribed BC absorption enhancement, and aerosol hygroscopicity, respectively. In each experiment, one factor was fixed at selected levels, and the CP sensitivities of the remaining factors were recalculated (Fig. 5). These experiments were designed to test the state dependence implied by the interaction analysis rather than to provide a single universal sensitivity ranking.

Under fixed surface albedo, the sensitivities of CT, BCPNSD, n_{shell}, k_{BC}, and PNSD changed clearly. This result indicates that the surface radiative boundary condition can regulate how aerosol microphysical perturbations are converted into changes in near-surface actinic flux. This interpretation is consistent with the role of surface albedo in controlling upwelling radiation and multiple scattering in photolysis-rate calculations (Walker et al., 2022). Therefore, the influence of aerosol microphysics on $J(NO_2)$ depends partly on surface reflection conditions.

Under fixed CT, the sensitivities of BCAE, BCPNSD, surface albedo, k_{BC}, and ρ_{BC} changed. This behaviour shows that the prescribed coating thickness modifies the relative sensitivities of BC size, density, and absorption-related factors. It is also consistent with the strong interaction between CT and BCAE shown in Sect. 3.3 and with previous studies showing that observed BC absorption enhancement varies with coating conditions, MS, and particle heterogeneity (Cappa et al., 2012; Liu et al., 2017; Fierce et al., 2016; Lan et al., 2024; Zeng et al., 2024).

Under fixed BCAE, the sensitivities of CT, surface albedo, BCPNSD, k_{BC}, and VD changed with the selected BCAE level. This indicates that the prescribed BCAE level modifies the relative sensitivities of coating thickness, surface reflection, BC size distribution, BC absorption, and aerosol vertical distribution. Since absorbing aerosols can reduce actinic flux and suppress photolysis under polluted conditions, changes in the prescribed BCAE level can alter how other aerosol factors influence $J(NO_2)$.

https://doi.org/10.5194/egusphere-2026-4877
Preprint. Discussion started: 21 September 2026

Under fixed κ, the sensitivities of surface albedo, CT, BCPNSD, PNSD, and RH varied, showing that hygroscopic growth modulates the response of size-distribution and humidity-related factors. This behaviour is consistent with the κ-Köhler description of water uptake and with previous work showing that aerosol hygroscopic growth can modify SSA and the $J(NO_2)$ response under humid conditions (Petters and Kreidenweis, 2007; Tao et al., 2014). These results indicate that κ not only acts as an individual factor but also regulates the pathway through which RH and particle size distribution affect optical properties and photolysis.

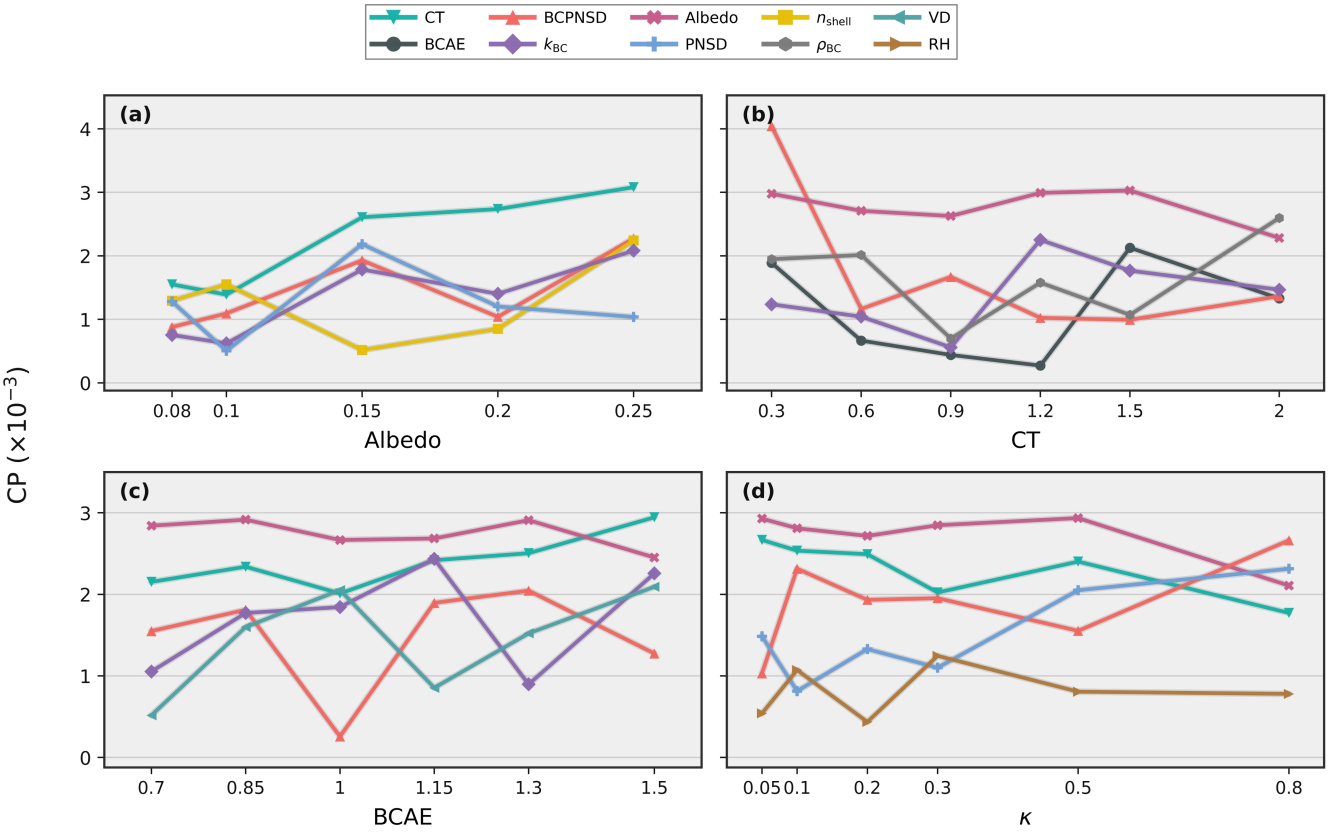

Figure 5. CP sensitivity of $J(NO_2)$ under fixed levels of key factors. Panels show results for fixed surface albedo, CT, BCAE, and κ. The horizontal axis gives the fixed level, and the vertical axis gives CP sensitivity.

These fixed-factor results support the interaction analysis by showing that the sensitivity of $J(NO_2)$ to one factor depends on the state of other key factors. Thus, the sensitivity ranking should be interpreted as state dependent rather than as a fixed ordering that applies to all aerosol and environmental conditions. Overall, the direct-input, aerosol microphysical, environmental, boundary-condition, interaction, and fixed-factor analyses consistently show that $J(NO_2)$ sensitivity is controlled by both direct optical properties and their underlying drivers. SSA and surface albedo are the dominant direct controls, while CT, ρ_{BC}, BCAE, k_{BC}, and κ represent important aerosol microphysical pathways. The interaction and fixed-

https://doi.org/10.5194/egusphere-2026-4877
Preprint. Discussion started: 21 September 2026

factor results further indicate that the sensitivity ranking is jointly modulated by coating thickness, BCAE, hygroscopic growth, and the surface radiative boundary condition.

https://doi.org/10.5194/egusphere-2026-4877
Preprint. Discussion started: 21 September 2026

4 Conclusions

$J(NO_2)$ is a central parameter in tropospheric photochemistry and ozone formation, and previous studies have shown that aerosol perturbations can substantially modify $J(NO_2)$. However, most existing sensitivity analyses of aerosol effects on $J(NO_2)$ have been conducted within OAT or OAT-type frameworks, in which individual aerosol optical, microphysical, environmental, or VD factors are perturbed separately. Such approaches mainly represent local single-factor responses and cannot fully resolve the co-variation, nonlinear responses, and interaction effects among aerosol optical properties, aerosol microphysical parameters, environmental conditions, and radiative-boundary factors. As a result, the sensitivity ranking and the key parameter combinations controlling $J(NO_2)$ remain uncertain. To address this issue, this study developed a new Mie–TUV framework incorporating the CP method to quantify the sensitivity of $J(NO_2)$ to aerosol optical properties and their related microphysical, environmental, and boundary-condition factors.

Using this framework, we first examined the direct radiative inputs to TUV, including AOD, SSA, g, and surface albedo. The results showed that SSA and surface albedo had the strongest sensitivities, indicating that $J(NO_2)$ is more strongly regulated by the scattering–absorption partitioning of aerosol extinction and by the lower radiative boundary condition than by column aerosol extinction alone. By contrast, AOD and g showed smaller sensitivities within the adopted parameter ranges, although they remain essential components of aerosol radiative inputs.

We then extended the analysis to aerosol microphysical, environmental, and boundary-condition factors through the Mie–TUV pathway. CT, ρ_{BC}, BCAE, the imaginary part of the BC refractive index, κ, and surface albedo were identified as important factors affecting $J(NO_2)$. These results suggest that aerosol effects on $J(NO_2)$ arise not only from total aerosol loading but also from variations in coating thickness, BCAE, aerosol hygroscopic growth, and surface reflection.

The interaction analysis further showed that $J(NO_2)$ sensitivity is not controlled by isolated factors alone. Differences between OAT and CP sensitivities indicate that nonlinear responses and factor coupling can modify the sensitivity ranking. The strongest interaction occurred between CT and BCAE, highlighting the need to jointly constrain coating thickness and BCAE. Fixed-factor experiments further showed that the relative importance of aerosol-related factors depends on the background state of key variables, especially surface albedo, CT, BCAE, and κ.

Overall, these findings highlight the need to better constrain SSA, surface albedo, CT, BCAE, κ, and VD in photolysis-frequency calculations. Such constraints are important for improving the representation of aerosol–photolysis interactions and for understanding the links between particulate matter and ozone pollution. The results should be interpreted within the limits of the present Mie–TUV framework, parameter ranges, and input data sources. Future work should combine more complete observations of aerosol optical and microphysical properties with photochemical or chemical-transport models to evaluate the broader impacts on atmospheric oxidation and secondary pollution.

https://doi.org/10.5194/egusphere-2026-4877
Preprint. Discussion started: 21 September 2026

Data availability

The MODIS AOD and surface albedo data used in this study are publicly available from the NASA MODIS data portal (https://modis.gsfc.nasa.gov/data/). The aerosol microphysical parameter settings adopted from previous studies are described and cited in the corresponding sections of the paper. The observational datasets from the Changping site used in this study are publicly available on Zenodo at https://doi.org/10.5281/zenodo.21042715. Any questions regarding the Changping datasets can be directed to the corresponding author, Gang Zhao (gangz@muc.edu.cn).

Code availability

The Python scripts used for data processing, model calculations, and figure generation are available from the corresponding author, Gang Zhao (gangz@muc.edu.cn), upon reasonable request.

Author contributions

Xinlei Lv designed the study, developed the method, performed the calculations, analysed the data, prepared the figures, and wrote the original manuscript. **Jie Sun** participated in the investigation, figure preparation, and manuscript revision. **Bishuo He** contributed to the Constrained Parameter method. **Fengjun Shen** participated in the investigation. **Gang Zhao** designed the study, provided resources, supervised the work, acquired funding, and revised the manuscript. **Tong Liu** participated in the investigation. **Qiqi Mo** participated in the investigation. **Linghan Zeng** contributed to method validation and manuscript revision. **Ziye Zhang** contributed to data curation. **Yunxiao Li** contributed to data curation. **Batu Alaxi** contributed to data curation. **Weili Lin** contributed to validation, supervision, and manuscript revision. **Chunsheng Zhao** contributed to validation, supervision, and manuscript revision.

AI tools statement

The authors used ChatGPT only for language editing, grammar checking, and improving the readability of parts of the manuscript. The tool was not used to generate scientific analyses, interpretations, results, or conclusions. All scientific content was developed, checked, and approved by the authors.

Competing interests

The contact author has declared that none of the authors has any competing interests.

https://doi.org/10.5194/egusphere-2026-4877
Preprint. Discussion started: 21 September 2026

Software

The data were processed using Python 3.8.5, and the figures were produced using Python 3.8.5.

Financial support

This study was financially supported by the National Key Research and Development Program of China (2023YFC3705300, Task 4), National Natural Science Foundation of China (grant no. 42405083).

References

An, Z., Huang, R.-J., Zhang, R., Tie, X., Li, G., Cao, J., Zhou, W., Shi, Z., Han, Y., Gu, Z., and Ji, Y.: Severe haze in northern China: A synergy of anthropogenic emissions and atmospheric processes, Proc. Natl. Acad. Sci. U.S.A., 116, 8657–8666, https://doi.org/10.1073/pnas.1900125116, 2019.

Bergstrom, R. W., Pilewskie, P., Russell, P. B., Redemann, J., Bond, T. C., Quinn, P. K., and Sierau, B.: Spectral absorption properties of atmospheric aerosols, Atmos. Chem. Phys., 7, 5937–5943, https://doi.org/10.5194/acp-7-5937-2007, 2007.

Bohren, C. F. and Huffman, D. R.: Absorption and Scattering of Light by Small Particles, Wiley, New York, 1983.

Burkholder, J. B., Sander, S. P., Abbatt, J., Barker, J. R., Cappa, C., Crounse, J. D., Dibble, T. S., Huie, R. E., Kolb, C. E., Kurylo, M. J., Orkin, V. L., Percival, C. J., Wilmouth, D. M., and Wine, P. H.: Chemical Kinetics and Photochemical Data for Use in Atmospheric Studies, Evaluation No. 19, JPL Publication 19-5, Jet Propulsion Laboratory, Pasadena, California, 2019.

Cappa, C. D., Onasch, T. B., Massoli, P., Worsnop, D. R., Bates, T. S., Cross, E. S., Davidovits, P., Hakala, J., Hayden, K. L., Jobson, B. T., Kolesar, K. R., Lack, D. A., Lerner, B. M., Li, S.-M., Mellon, D., Nuaaman, I., Olfert, J. S., Petaja, T., Quinn, P. K., Song, C., Subramanian, R., Williams, E. J., and Zaveri, R. A.: Radiative absorption enhancements due to the mixing state of atmospheric black carbon, Science, 337, 1078–1081, https://doi.org/10.1126/science.1223447, 2012.

Chen, H., Zhuang, B., Liu, J., Zhou, Y., Hu, Y., Chen, Y., Gao, Y., Wei, W., Lin, H., Li, S., Wang, T., Xie, M., and Li, M.: Absorbing aerosol optical properties and radiative effects on near-surface photochemistry in East Asia, Remote Sens., 15, 2779, https://doi.org/10.3390/rs15112779, 2023.

Chen, X., Li, K., Yang, T., Jin, X., Chen, L., Yang, Y., Zhao, S., Hu, B., Zhu, B., Wang, Z., and Liao, H.: Simulated photochemical response to observational constraints on aerosol vertical distribution over North China, Atmos. Chem. Phys., 25, 9151–9168, https://doi.org/10.5194/acp-25-9151-2025, 2025.

Doherty, S. J., Saide, P. E., Zuidema, P., Shinozuka, Y., Ferrada, G. A., Gordon, H., Mallet, M., Meyer, K., Painemal, D., Howell, S. G., Freitag, S., Dobracki, A., Podolske, J. R., Burton, S. P., Ferrare, R. A., Howes, C., Nabat, P., Carmichael, G. R., da Silva, A., Pistone, K., Chang, I., Gao, L., Wood, R., and Redemann, J.: Modeled and observed properties related to the direct aerosol radiative effect of biomass burning aerosol over the southeastern Atlantic, Atmos. Chem. Phys., 22, 1–46, https://doi.org/10.5194/acp-22-1-2022, 2022.

https://doi.org/10.5194/egusphere-2026-4877
Preprint. Discussion started: 21 September 2026

Fierce, L., Bond, T. C., Bauer, S. E., Mena, F., and Riemer, N.: Black carbon absorption at the global scale is affected by particle-scale diversity in composition, Nat. Commun., 7, 12361, https://doi.org/10.1038/ncomms12361, 2016.

Frey, H. C. and Patil, S. R.: Identification and review of sensitivity analysis methods, Risk Anal., 22, 553 – 578, https://doi.org/10.1111/0272-4332.00039, 2002.

Gao, J., Li, Y., Xie, Z., Wang, L., Hu, B., and Bao, F.: Which aerosol type dominate the impact of aerosols on ozone via changing photolysis rates?, Sci. Total Environ., 854, 158580, https://doi.org/10.1016/j.scitotenv.2022.158580, 2023.

Gerasopoulos, E., Kazadzis, S., Vrekoussis, M., Kouvarakis, G., Liakakou, E., Kouremeti, N., Giannadaki, D., Kanakidou, M., Bohn, B., and Mihalopoulos, N.: Factors affecting O_3 and NO_2 photolysis frequencies measured in the eastern Mediterranean during the five-year period 2002–2006, J. Geophys. Res.-Atmos., 117, D22305, https://doi.org/10.1029/2012JD017622, 2012.

He, B. and Zhao, C.: A novel method to quantify the uncertainty contribution of aerosol–radiation interaction factors, Atmos. Chem. Phys., 25, 7765–7776, https://doi.org/10.5194/acp-25-7765-2025, 2025.

He, C., Liu, J., Zhou, Y., Zhou, J., Zhang, L., Wang, Y., Liu, L., and Peng, S.: Synergistic $PM_{2.5}$ and O_3 control to address the emerging global $PM_{2.5}$ – O_3 compound pollution challenges, Eco-Environment & Health, 3, 325 – 337, https://doi.org/10.1016/j.eehl.2024.04.004, 2024.

He, S. and Carmichael, G. R.: Sensitivity of photolysis rates and ozone production in the troposphere to aerosol properties, J. Geophys. Res.-Atmos., 104, 26307–26324, https://doi.org/10.1029/1999JD900789, 1999.

Huang, R.-J., Zhang, Y., Bozzetti, C., Ho, K.-F., Cao, J.-J., Han, Y., Daellenbach, K. R., Slowik, J. G., Platt, S. M., Canonaco, F., Zotter, P., Wolf, R., Pieber, S. M., Bruns, E. A., Crippa, M., Ciarelli, G., Piazzalunga, A., Schwikowski, M., Abbaszade, G., Schnelle-Kreis, J., Zimmermann, R., An, Z., Szidat, S., Baltensperger, U., El Haddad, I., and Prévôt, A. S. H.: High secondary aerosol contribution to particulate pollution during haze events in China, Nature, 514, 218 – 222, https://doi.org/10.1038/nature13774, 2014.

Kayetha, V., Torres, O., and Jethva, H.: Retrieval of UV−visible aerosol absorption using AERONET and OMI−MODIS synergy: spatial and temporal variability across major aerosol environments, Atmos. Meas. Tech., 15, 845 – 877, https://doi.org/10.5194/amt-15-845-2022, 2022.

Lan, Y., Huang, X., Li, G., Hu, W., Zhu, Q., Zeng, L., and Hu, M.: Light absorption enhancement of black carbon and its impact factors during winter in a megacity of the Sichuan Basin, China, Sci. Total Environ., 922, 171224, https://doi.org/10.1016/j.scitotenv.2024.171224, 2024.

Lee, L. A., Carslaw, K. S., Pringle, K. J., Mann, G. W., and Spracklen, D. V.: Emulation of a complex global aerosol model to quantify sensitivity to uncertain parameters, Atmos. Chem. Phys., 11, 12253–12273, https://doi.org/10.5194/acp-11-12253-2011, 2011.

Lee, L. A., Reddington, C. L., and Carslaw, K. S.: On the relationship between aerosol model uncertainty and radiative forcing uncertainty, Proc. Natl. Acad. Sci. U.S.A., 113, 5820–5827, https://doi.org/10.1073/pnas.1507050113, 2016.

https://doi.org/10.5194/egusphere-2026-4877
Preprint. Discussion started: 21 September 2026

572 Levy, R. C., Mattoo, S., Munchak, L. A., Remer, L. A., Sayer, A. M., Patadia, F., and Hsu, N. C.: The Collection 6 MODIS
573 aerosol products over land and ocean, Atmos. Meas. Tech., 6, 2989–3034, https://doi.org/10.5194/amt-6-2989-2013, 2013.
574 Li, C., Zhao, S., Wu, S., Liu, K., and Hu, B.: Characterisation of long-term changes in photolysis rate in Beijing based on
575 observation and simulation, Plateau Meteorology, 44, 1645–1655, https://doi.org/10.7522/j.issn.1000-0534.2025.00037, 2025.
576 Li, G., Zhang, R., Fan, J., and Tie, X.: Impacts of black carbon aerosol on photolysis and ozone, J. Geophys. Res.-Atmos., 110,
577 D23206, https://doi.org/10.1029/2005JD005898, 2005.
578 Liu, D., Whitehead, J., Alfarra, M. R., Reyes-Villegas, E., Spracklen, D. V., Reddington, C. L., Kong, S., Williams, P. I., Ting,
579 Y.-C., Haslett, S., Taylor, J. W., Flynn, M. J., Morgan, W. T., McFiggans, G., Coe, H., and Allan, J. D.: Black-carbon
580 absorption enhancement in the atmosphere determined by particle mixing state, Nat. Geosci., 10, 184 – 188,
581 https://doi.org/10.1038/ngeo2901, 2017.
582 Liu, J., Niu, X., Zhang, L., Yang, X., Zhao, P., and He, C.: Exposure risk assessment and synergistic control pathway
583 construction for O_3 – $PM_{2.5}$ compound pollution in China, Atmos. Environ.: X, 21, 100240,
584 https://doi.org/10.1016/j.aeaoa.2024.100240, 2024.
585 Loeb, N. G. and Su, W.: Direct aerosol radiative forcing uncertainty based on a radiative perturbation analysis, J. Clim., 23,
586 5288–5293, https://doi.org/10.1175/2010JCLI3543.1, 2010.
587 Ma, X., Huang, J., Zhao, T., Liu, C., Zhao, K., Xing, J., and Xiao, W.: Rapid increase in summer surface ozone over the North
588 China Plain during 2013 – 2019: a side effect of particulate matter reduction control?, Atmos. Chem. Phys., 21, 1 – 16,
589 https://doi.org/10.5194/acp-21-1-2021, 2021.
590 Madronich, S. and Flocke, S.: The role of solar radiation in atmospheric chemistry, in: Environmental Photochemistry, The
591 Handbook of Environmental Chemistry, vol. 2/2L, edited by: Boule, P., Springer, Berlin, Heidelberg, 1 – 26,
592 https://doi.org/10.1007/978-3-540-69044-3_1, 1999.
593 McComiskey, A., Schwartz, S. E., Schmid, B., Guan, H., Lewis, E. R., Ricchiazzi, P., and Ogren, J. A.: Direct aerosol forcing:
594 Calculation from observables and sensitivities to inputs, J. Geophys. Res.-Atmos., 113, D09202,
595 https://doi.org/10.1029/2007JD009170, 2008.
596 Moosmüller, H. and Chakrabarty, R. K.: Technical Note: Simple analytical relationships between Ångström coefficients of
597 aerosol extinction, scattering, absorption, and single scattering albedo, Atmos. Chem. Phys., 11, 10677 – 10680,
598 https://doi.org/10.5194/acp-11-10677-2011, 2011.
599 Morris, M. D.: Factorial sampling plans for preliminary computational experiments, Technometrics, 33, 161 – 174,
600 https://doi.org/10.1080/00401706.1991.10484804, 1991.
601 Petters, M. D. and Kreidenweis, S. M.: A single parameter representation of hygroscopic growth and cloud condensation
602 nucleus activity, Atmos. Chem. Phys., 7, 1961–1971, https://doi.org/10.5194/acp-7-1961-2007, 2007.

https://doi.org/10.5194/egusphere-2026-4877
Preprint. Discussion started: 21 September 2026

Russell, P. B., Bergstrom, R. W., Shinozuka, Y., Clarke, A. D., DeCarlo, P. F., Jimenez, J. L., Livingston, J. M., Redemann, J., Dubovik, O., and Strawa, A.: Absorption Angstrom Exponent in AERONET and related data as an indicator of aerosol composition, Atmos. Chem. Phys., 10, 1155–1169, https://doi.org/10.5194/acp-10-1155-2010, 2010.

Saltelli, A., Tarantola, S., and Chan, K.-S.: A quantitative model-independent method for global sensitivity analysis of model output, Technometrics, 41, 39–56, https://doi.org/10.1080/00401706.1999.10485594, 1999.

Saltelli, A., Ratto, M., Tarantola, S., and Campolongo, F.: Sensitivity analysis for chemical models, Chem. Rev., 105, 2811–2828, https://doi.org/10.1021/cr040659d, 2005.

Schaaf, C. B., Gao, F., Strahler, A. H., Lucht, W., Li, X., Tsang, T., Strugnell, N. C., Zhang, X., Jin, Y., Muller, J.-P., Lewis, P., Barnsley, M., Hobson, P., Disney, M., Roberts, G., Dunderdale, M., Doll, C., d'Entremont, R. P., Hu, B., Liang, S., Privette, J. L., and Roy, D.: First operational BRDF, albedo nadir reflectance products from MODIS, Remote Sens. Environ., 83, 135–148, https://doi.org/10.1016/S0034-4257(02)00091-3, 2002.

Shetter, R. E., Cinquini, L., Lefer, B. L., Hall, S. R., and Madronich, S.: Comparison of airborne measured and calculated spectral actinic flux and derived photolysis frequencies during the PEM-Tropics B mission, J. Geophys. Res.-Atmos., 108, 8234, https://doi.org/10.1029/2001JD001320, 2003.

Tao, J. C., Zhao, C. S., Ma, N., and Liu, P. F.: The impact of aerosol hygroscopic growth on the single-scattering albedo and its application on the NO_2 photolysis rate coefficient, Atmos. Chem. Phys., 14, 12055–12067, https://doi.org/10.5194/acp-14-12055-2014, 2014.

Thorsen, T. J., Ferrare, R. A., Kato, S., and Winker, D. M.: Aerosol direct radiative effect sensitivity analysis, J. Clim., 33, 6119–6139, https://doi.org/10.1175/JCLI-D-19-0669.1, 2020.

Trebs, I., Bohn, B., Ammann, C., Rummel, U., Blumthaler, M., Königstedt, R., Meixner, F. X., Fan, S., and Andreae, M. O.: Relationship between the NO_2 photolysis frequency and the solar global irradiance, Atmos. Meas. Tech., 2, 725 – 739, https://doi.org/10.5194/amt-2-725-2009, 2009.

Walker, H. L., Heal, M. R., Braban, C. F., Whalley, L. K., and Twigg, M. M.: Evaluation of local measurement-driven adjustments of modelled cloud-free atmospheric photolysis rate coefficients, Environ. Sci.: Atmos., 2, 1411 – 1427, https://doi.org/10.1039/D2EA00072E, 2022.

Wang, W., Li, X., Shao, M., Hu, M., Zeng, L., Wu, Y., and Tan, T.: The impact of aerosols on photolysis frequencies and ozone production in Beijing during the 4-year period 2012 – 2015, Atmos. Chem. Phys., 19, 9413 – 9429, https://doi.org/10.5194/acp-19-9413-2019, 2019.

Zeng, L., Tan, T., Zhao, G., Du, Z., Liu, Q., Li, J., Wu, C., Wang, Y., Liu, D., Song, Y., Wang, Q., Deng, W., Hu, M., and Zhu, T.: Overestimation of black carbon light absorption due to mixing state heterogeneity, npj Clim. Atmos. Sci., 7, 2, https://doi.org/10.1038/s41612-023-00535-8, 2024.

https://doi.org/10.5194/egusphere-2026-4877
Preprint. Discussion started: 21 September 2026

634 Zhao, G., Zhao, C. S., Kuang, Y., Bian, Y., Tao, J., Shen, C., and Yu, Y.: Calculating the aerosol asymmetry factor based on
635 measurements from the humidified nephelometer system, Atmos. Chem. Phys., 18, 9049–9060, https://doi.org/10.5194/acp-
636 18-9049-2018, 2018.
637 Zhao, S., Yu, Y., Qin, D., Yin, D., Dong, L., He, J., Liu, N., Yu, C., and Xiao, J.: The influence of aerosols on the NO_2
638 photolysis rate in a suburban site in North China, Sci. Total Environ., 767, 144788,
639 https://doi.org/10.1016/j.scitotenv.2020.144788, 2021.